frontiers | Frontiers in Earth Science

TYPE Original Research
PUBLISHED 10 May 2023
DOI 10.3389/feart.2023.1206835

OPEN ACCESS

EDITED BY
George Kontakiotis,
National and Kapodistrian University of Athens, Greece

REVIEWED BY
Ruoyuan Qiu,
institute of geology and geophysics, China
Yang Li,
Shandong University of Science and Technology, China

*CORRESPONDENCE
Rui Zhang,
ruizhangxu@pku.edu.cn

RECEIVED 16 April 2023
ACCEPTED 02 May 2023
PUBLISHED 10 May 2023

CITATION
Liu G, Zhang R, He X, Wei R, Zhu R, Tang Y, He W, Zheng M, Chang Q, Wang R and Zhao X (2023), Cyclostratigraphy and high-frequency sedimentary cycle framework for the Late Paleozoic Fengcheng Formation, Junggar Basin. *Front. Earth Sci.* 11:1206835. doi: 10.3389/feart.2023.1206835

Cyclostratigraphy and high-frequency sedimentary cycle framework for the Late Paleozoic Fengcheng Formation, Junggar Basin

Guoyong Liu[1], Rui Zhang[2,3]*, Xiangwu He[2,3], Ren Wei[2,3], Rukai Zhu[2,4], Yong Tang[1], Wenjun He[1], Menglin Zheng[1], Qiusheng Chang[1], Ran Wang[1] and Xinmei Zhao[1]

[1]PetroChina Xinjiang Oilfield Company, Karamay, China, [2]Institute of Energy, Peking University, Beijing, China, [3]State Key Laboratory of Shale Oil and Gas Enrichment Mechanisms and Effective Development, Sinopec, Beijing, China, [4]PetroChina Research Institute of Petroleum Exploration and Development, Beijing, China

The Late Paleozoic Fengcheng Formation within the Mahu Sag of the Junggar Basin (China) harbors the world's oldest alkaline lake hydrocarbon source rocks. Spectral analysis of the natural gamma-ray (GR) series obtained from four boreholes traversing the Fengcheng Formation, with wavelength ranges of 28.4 m–50 m, 5.9 m–12.6 m, 2.3 m–3.9 m, and 1.2 m–2.7 m. These were controlled by Early Permian astronomical cycles, including 405 kyr long eccentricity, 100 kyr short eccentricity, 34.2 kyr obliquity, and 20.7–17.4 kyr precession. The most significant cycle was notably that of the 405 kyr long eccentricity, which was instrumental for dividing and correlating the high-frequency sedimentary sequences in lacustrine shales. Nine intermediate-term and 36 short-term base-level cycles were identified in the P_1f_1 and P_1f_2 members of the Fengcheng Formation. These cycle types are equal to the 405 kyr long eccentricity cycle and ~100 kyr short eccentricity cycle, respectively. The paleolake-level variations in the Fengcheng Formation were reconstructed using sedimentary noise modeling, revealing that lake levels reached their highest value during the deposition of the P_1f_2 Member. The spatial distribution patterns of lithofacies in the Fengcheng Formation can be clearly demonstrated within the isochronous cycle framework under the constraints of long eccentricity cycles. The use of astronomical cycles in isochronous stratigraphic correlation offers great potential for characterizing alkaline lacustrine sequences and predicting favorable areas for shale oil exploration with higher accuracy.

KEYWORDS

Milankovitch cycles, Mahu Sag, alkaline lacustrine, lake-level variations, isochronous stratigraphic correlation, cyclostratigraphy

1 Introduction

The sedimentary geological record preserves patterns of repetitive sedimentary cycles (Weedon, 2003; Kodama and Hinnov, 2014). According to cyclostratigraphy theory, rhythmic features in the sedimentary record worldwide are indicative of past climate signatures related to variations in the total solar insolation encountered on the surface

of the Earth owing to quasiperiodic parameter variabilities in the planet's orbit (Boulila et al., 2011; Hinnov and Hilgen, 2012; Eldrett et al., 2015). Previous studies have derived a link between cyclostratigraphy and an astronomical time scale (ATS) by modeling the stratigraphic records of such cycles with astronomical solutions (Laskar et al., 2004; Waltham, 2015). For example, successful orbital tuning in eastern North America's Newark rift basin has revealed a wide range of lake-level changes related to precession periods (Olsen and Kent, 1996; Kent et al., 2017). Liu et al. (2022) established a floating timeline that was calibrated to the long eccentricity cycles (405 kyr) and redefined the high-resolution marine sequence framework of the organic-rich Qiongzhusi shale of Early Cambrian age in the Sichuan Basin.

The development of terrestrial basin sedimentary sequences is controlled by climate cycling driven by the Earth's orbital cycles (Du et al., 2020; Huang et al., 2021; Wu et al., 2022). The continuity and stability of fine-grained lacustrine deposits around the world have been clearly demonstrated to be linked to the Milankovitch cycle (Olsen and Kent, 1996; Meyers, 2019; Fang et al., 2023). The division of high-frequency shale-series cycles helps to clarify the spatiotemporal characteristics of organic-rich shale distributions, thereby providing a foundation for the development of shale oil and gas exploration. However, deep shale deposits show a uniform structure, which makes it difficult to identify key sequence interfaces. Identifying the Milankovitch cycle within the strata has allowed sedimentary cycles to be divided with time connotations and isochronous correlations with regional and even global stratigraphic sequences (Zhang et al., 2019; Wei et al., 2023). The sedimentary rhythm of calcium sulfate in the Permian Castile and Bell Canyon Formations of the Delaware Basin records an average period of ~20 kyr precession (Anderson, 1982). The evaporite-rich stratigraphic sequence of the Qianjiang Formation in the Jianghan Basin also records lake cycles alternating between saline water and fresh water in pace with orbital eccentricity cycles on an ~100-kyr timescale (Huang and Hinnov, 2019).

The Fengcheng Formation is a Lower Permian stratigraphic sequence within the Mahu Sag in the Junggar Basin that contains the oldest alkaline lake hydrocarbon source rocks on Earth (Zhang et al., 2018; Huang et al., 2021; Tang et al., 2022). Although previous studies have reported climatically forced evaporite-containing sediments (Cao et al., 2020), the detailed relationships between alkaline lacustrine development and orbital forcing remain to be determined. This can mainly be explained by the low resolution of the age framework and absence of a higher-resolution and reliable paleoclimate model for the Fengcheng Formation, thereby making it challenging to constrain the essential mechanisms that power the hydrological processes responsible for evaporite formation in this region. To address this question, we conducted cyclostratigraphic analyses of lacustrine deposits in the Early Permian Fengcheng Formation using logs of gamma-ray (GR) spectra from four boreholes. The primary purposes of this work are as follows: 1) to determine the prominent depositional cycles and to construct a floating ATS for the Fengcheng Formation; 2) to reconstruct the Early Permian lake-level changes during the Fengcheng Formation's deposition; and 3) to categorize a high-frequency sedimentary cycle framework for the Fengcheng Formation using the periodic filtering curves of orbital parameters. This study therefore provides a typical case study for delineating high-frequency sequences in terrestrial black shales and serves as a valuable reference for predicting the distribution of shale oil deposits in alkaline–lacustrine basins.

2 Geological setting

Located in northwestern China (~45°N, 85°E), the Junggar Basin is a huge inland lake basin that is tectonically constricted by the Hala'alate and Zhayier Mountains to the northwest, the Kelamaili Mountains to the northeast, and the Bogda Mountains to the south (Figures 1A, B). Within the Junggar Basin, an approximately 1.5-km-thick stratigraphic sequence adequately documents important long-term features of the tectonic evolution of Central Asia, in addition to the evolution of paleoclimate and paleoenvironmental conditions of the continental region at middle to high latitudes in the Northern Hemisphere from the Paleozoic to the Cenozoic (Huang et al., 2021; Tang et al., 2022). With its location in the northwestern part of the Junggar Basin, the Mahu Sag is a major oil-bearing depression of approximately 5,000 km^2 in area (Yu et al., 2018b). The Zhongguai uplift and Wu-Xia and Ke-Bai fault zones (from south to north) occur in the Mahu Sag's western region, while the Dabasong, Xiayan, and Sangequan uplifts, Yingxi Sag, and Shiyingtan uplift (from south to north) occur in the eastern part (Figure 1C). However, the depositional processes and stratigraphic correlations within the depression remain difficult to understand due to complex tectonic deformation (Yu et al., 2018a).

The Fengcheng Formation mostly contains a mixture of fine-grained deposits from multiple sources in a moderately deep to deep alkaline lake setting and includes endogenous chemical deposits derived from a hot arid climate, rapid accumulation of fan deltaic clastic debris from the proximal end, and volcanic material sourced from peripheral volcanism during the evolution of the foreland basin, which was distributed throughout the generally margin area of the sag (Kuang et al., 2012; Zhi et al., 2021). In terms of classification, the Fengcheng Formation has been divided from bottom to top into P_1f_1, P_1f_2, and P_1f_3 members (Cao et al., 2020; Huang et al., 2021; Song et al., 2022). Recent exploration has shown that the depositional mixture of endogenous carbonates, volcanic material, and terrigenous clasts in the Fengcheng Formation produced a variety of lithotypes, such as salt rock, dolomite, mudstone, conglomerate, sandstone, tuff, and various transitional lithologies (Zhang et al., 2018). The lower member (P_1f_1) mainly consists of ignimbrite, coarse clastic rocks, mafic-intermediate volcanic rocks, and tuffs. The second member (P_1f_2) contains rhythmic evaporites, bedded dolomite, and lower volcanic with thicknesses ranging from 217 to 650 m. Moreover, alkaline minerals (e.g., searlesite, reedmergnerite, eitelite, wegscheiderite) are commonly distributed in this stratigraphic unit. The third member (P_1f_3) is dominantly characterized by mudstones containing terrigenous clastics in the upper section and dolomitic mudstones in the lower section (Cao et al., 2020; Wang et al., 2021).

Wells MY-1, XY-1, X-203, and M-49 are situated in the Wu-Xia fault zone in the Junggar Basin's western uplift. These are standard wells for exploring alkaline lacustrine shale oil in the Mahu Sag. Among them, the MY-1 borehole obtained complete geological archives regarding the Fengcheng Formation's sedimentary evolution by continuously coring more than 300 m. The P_1f_1

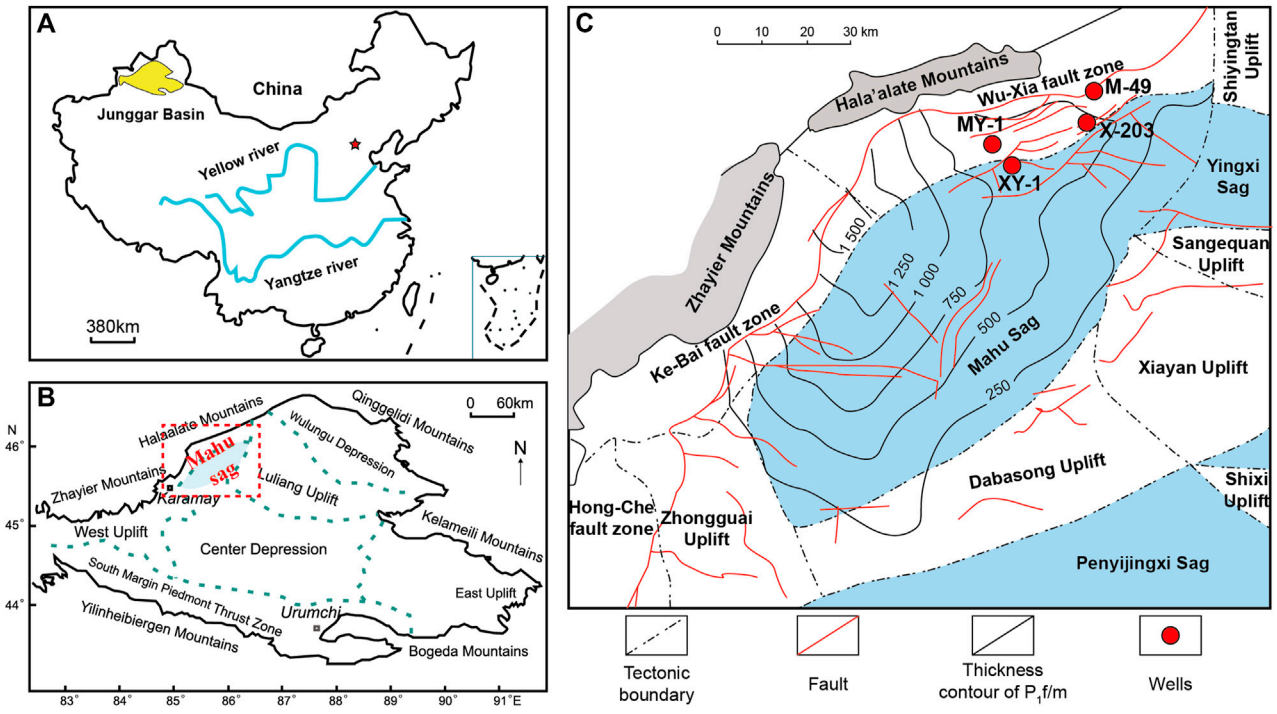

FIGURE 1
Geological setting of the Mahu Sag in the Junggar Basin (Huang et al., 2021; Wang et al., 2022). **(A)** Location of the Junggar Basin in China. **(B)** Mahu Sag and other tectonic units of the Junggar Basin. **(C)** Tectonic characteristics of the Mahu Sag and drill holes selected in this study.

Member in the MY-1 borehole comprises fine tuffaceous sandstone and gray dolomitic mudstone. The lower portion of the P_1f_1 Member is made up of pyroclastic sediment containing volcanic lithology, while the upper portion contains dolomitic rocks and organic-rich mudstone. The P_1f_2 Member contains dark gray mudstone intercalated with dolomitic mudstone, which was deposited in an evaporitic environment that contained a limited amount of clastic grains. The P_1f_3 Member comprises silty mudstone, dolomitic mudstone, and grayish-black lime mudstone. The lithological features of the other three boreholes are comparable to those of the MY-1 borehole, except for the large sets of alkaline mineral-enriched sections and dolomitic rocks in the P_1f_1 Member of the XY-1 and X-203 wells (Figure 2). Gypsum salt rocks pose a significant challenge to cyclostratigraphic analysis; volcanic rocks and tuff layers were excluded from the time series studies because they represent instantaneous events (e.g., Eldrett et al., 2015). The P_1f_1 and P_1f_2 members of the Fengcheng Formation are therefore the primary targets of our isochronous cycle framework.

3 Materials and methods

3.1 GR series

GR series are extensively used for time-series analysis owing to their high data acquisition efficiency and relatively clear lithologic variability characteristics (Li et al., 2019b; Zhang et al., 2019). Spectra from the four wells were used in this study for cyclostratigraphic analysis. The GR series reflects concentrations of uranium, thorium, and potassium (K). Lower GR values are generally associated with sandstone or carbonate-rich sediments, while higher values are typically linked with clay-rich sediments (Wang et al., 2020; Huang et al., 2021; Wei et al., 2023). Organic and clay mineral-rich sediments deposited in lake basins are known to be highly sensitive to paleoclimate and paleoenvironmental variations; GR series proxy can therefore be used as a raw signal associated with paleoclimate changes. Another feature of the GR series proxy is its higher signal-to-noise ratios than other similar proxies, which makes it a widely used tool in cyclostratigraphic studies (Wu et al., 2013; Li et al., 2019b; Huang et al., 2020; Wang et al., 2020). Overall, wet and warm depositional intervals are generally related to increased input of muddy components, which produces higher GR values, while dry and warm depositional intervals are generally linked with reduced inputs, thereby producing lower GR values. The periodic oscillations in the GR dataset are therefore a favorable proxy for the astronomical causes of climate variations in lacustrine basins (van Vugt et al., 2001; Huang and Hinnov, 2019).

3.2 Time series analysis methods

A quantitative approach to cyclostratigraphy is required to distinguish astronomical signals from spectra. This work applied a multitaper method (MTM) (Thomson, 1982; Mann and Lees, 1996) using *Acycle* v2.0 software (Li et al., 2019a). Before the analysis, the GR series were rescaled at 12.5-cm intervals to acquire unified data using linear interpolation. The removal of long-term trends from the

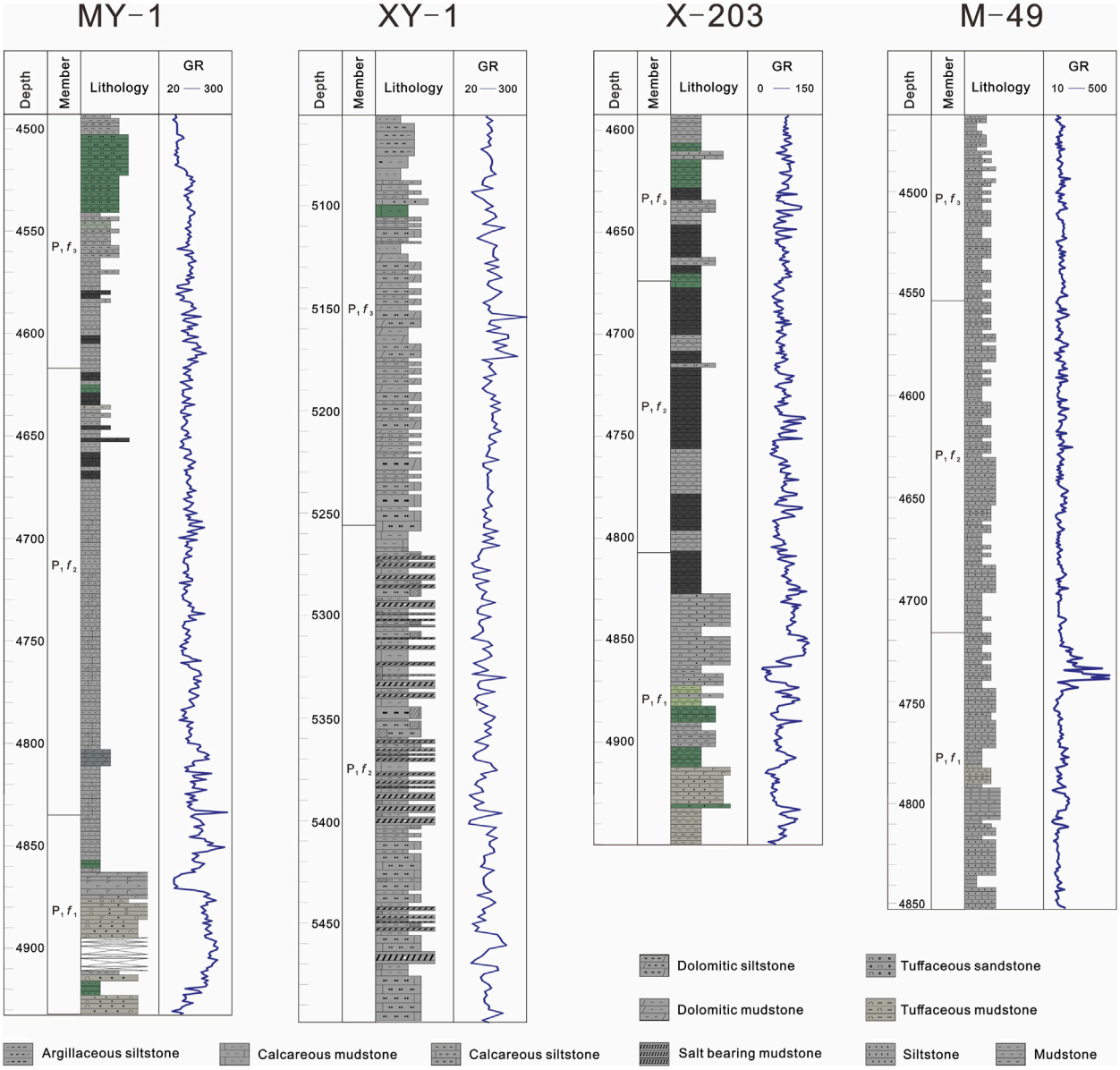

FIGURE 2
Lithological log and GR profile of well sections along the provenance direction, including wells MY-1, XY-1, X-203, and M-49.

original GR series was required to minimize distortion of the spectra's low-frequency section using the "rLOWESS" method (smoother = 20%–35%) (Cleveland, 1979). Logarithmic transformation is a common data preprocessing technique to reduce the range of data and reduce the effect of outliers when the range of values of the GR series is too large. The MTM assesses spectra obtained from detrended GR series using three 2π tapers. Gaussian bandpass filters are used to obtain interpreted signals from the GR series involving Milankovitch components (Li et al., 2019a). The significance of the rejected null AR1 models in all of the spectral analyses was calculated at confidence levels of 90%, 95%, and 99%. An evolving fast Fourier transform (FFT) spectrogram was used to investigate the frequency variations (Kodama and Hinnov, 2014).

The correlation coefficient (COCO) method can be applied to estimate the correlation coefficient between an astronomical solution and a GR series' power spectrum in the depth domain, thereby transforming the raw GR spectra from the depth measurements into a serial test of sedimentation rate in the time domain. The most plausible sedimentation rate is assumed to correspond to the maximum correlation coefficient. The evolutionary correlation coefficient method (eCOCO) has been adapted to trace variable sedimentation rates using both the COCO and running window methods (Li et al., 2018b; Wang et al., 2020; Wei et al., 2023). All of the analysis steps were performed using *Acycle* v2.0 software (Li et al., 2019a).

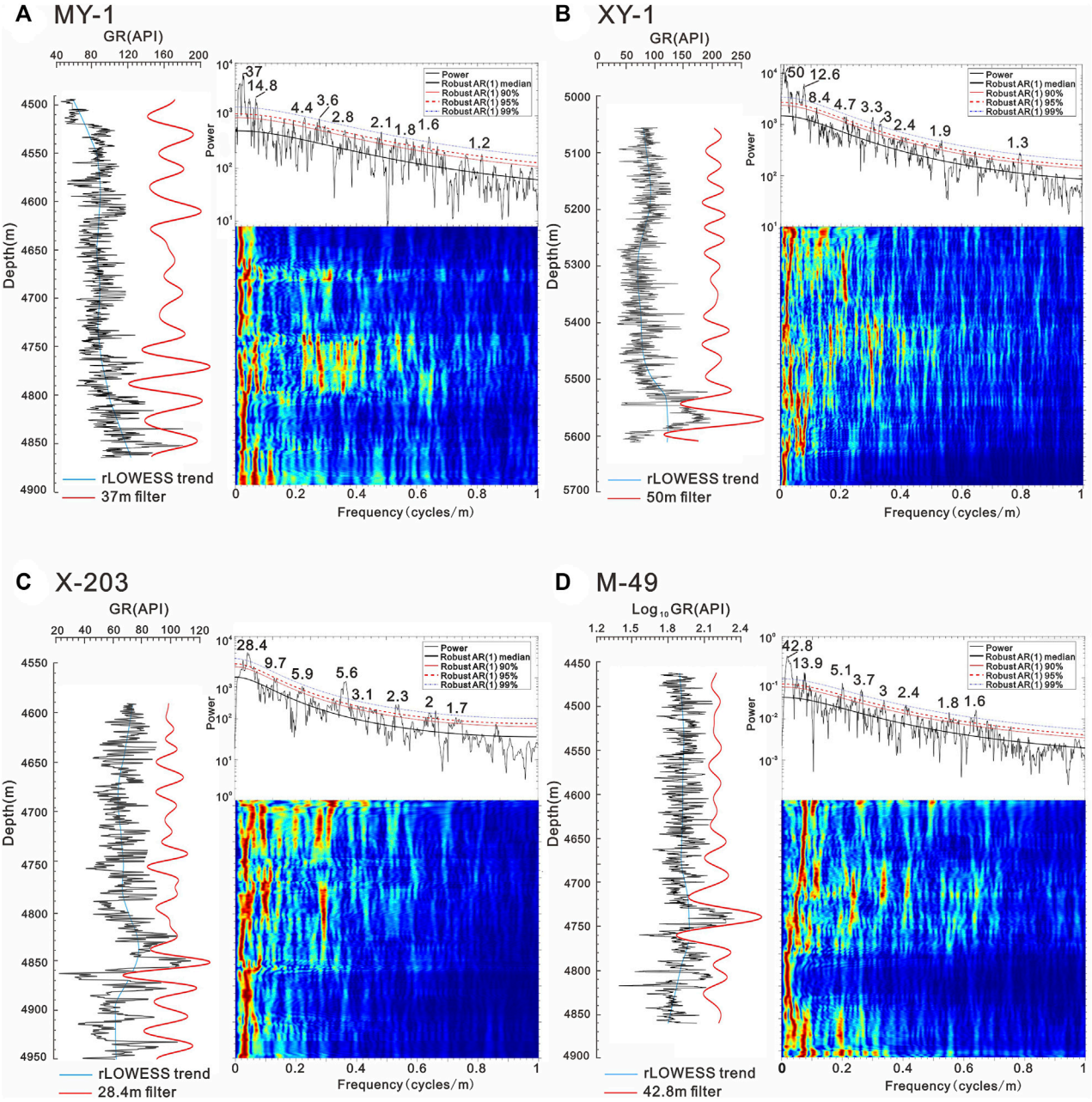

FIGURE 3
Cyclostratigraphic interpretation from wells MY-1, XY-1, X-203, and M-49 in the depth (m) domain of the Fengcheng Formation. Black curves are original GR series with 20%–35% weighted average rLOWESS trend (blue curve). The sedimentary cycles that are interpreted to be forced by the 405-kyr orbital eccentricity cycles are shown in red. **(A)** The evolutionary FFT spectrograms and 2π MTM power spectra of the untuned GR series show filter outputs at 37 m (0.027 ± 0.01 cycles/m) for well MY-1. **(B)** The evolutionary FFT spectrograms and 2π MTM power spectra of the untuned GR series show filter outputs at 50 m (0.020 ± 0.01 cycles/m) for well XY-1. **(C)** The evolutionary FFT spectrograms and 2π MTM power spectra of the untuned GR series show filter outputs at 28.4 m (0.035 ± 0.01 cycles/m) for well X-203. **(D)** The evolutionary FFT spectrograms and 2π MTM power spectra of the untuned GR series show filter outputs at 42.8 m (0.023 ± 0.01 cycles/m) for well M-49.

3.3 Lag-1 autocorrelation coefficient (ρ_1) model

Li et al. (2018a) proposed a sedimentary noise modeling method that provides a new approach to studying the variations in ancient sea-levels. Paleoclimate changes tend to incorporate prior values over a certain time frame, which is referred to as persistence or autocorrelation. The most commonly used persistence model is developed based on the lag-1 autocorrelation coefficient (ρ_1) (Mudelsee, 2002; Meyers and Hinnov, 2010; Li et al., 2018a), which is given as (Mudelsee, 2002):

$$\rho_1 = \frac{\sum_{i=2}^{n} x_{(i)}{}^{*} x_{(i-1)}}{\sum_{i=2}^{n} x_{(i-1)}^2} \quad (1)$$

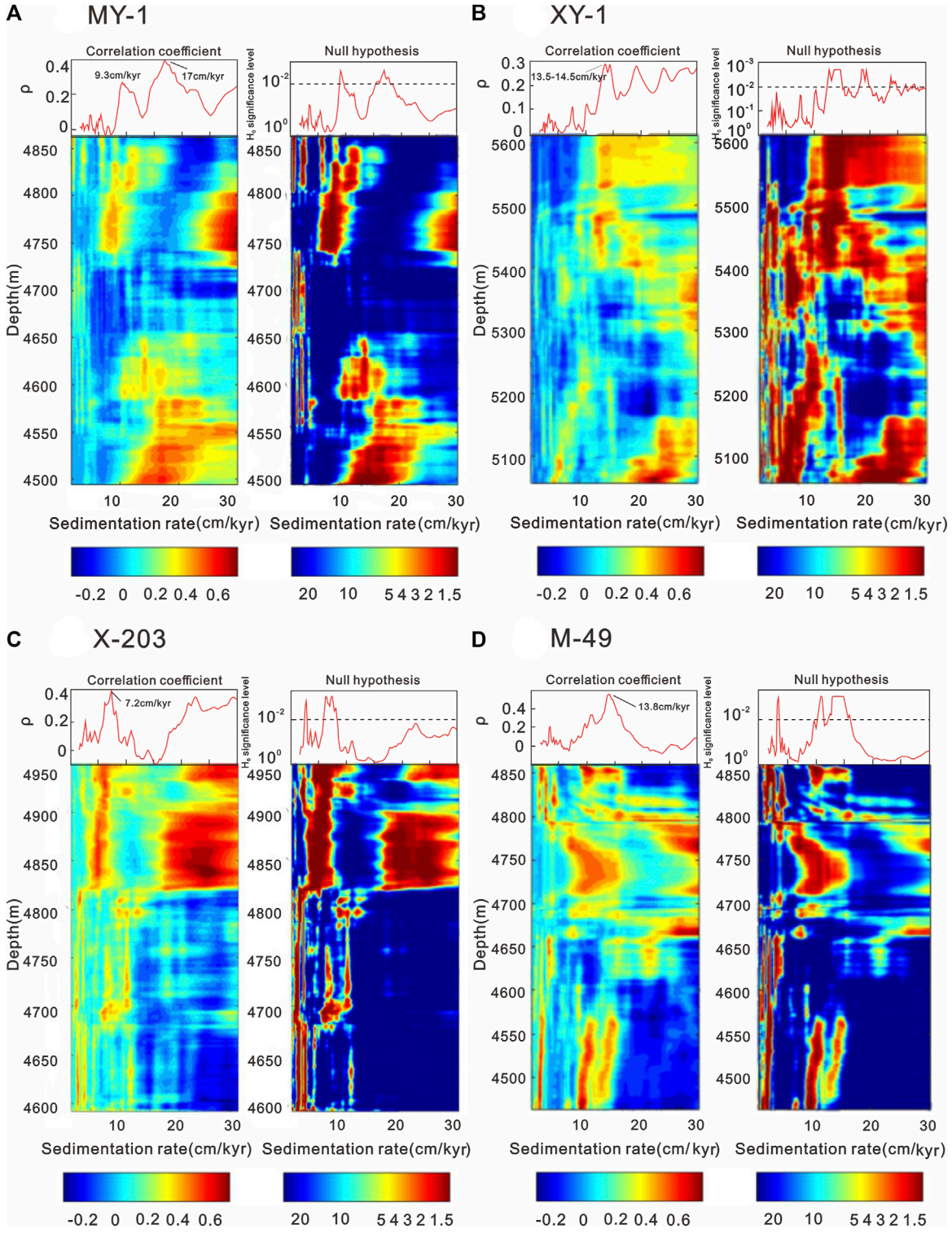

FIGURE 4
The COCO and eCOCO sedimentation rate map of the GR series of the Fengcheng Formation from wells MY-1 **(A)**, XY-1 **(B)**, X-203 **(C)**, and M-49 **(D)**. For the eCOCO analysis, the number of Monte Carlo simulations is 2,000; the sliding window is 70 m with a sliding window step of 1 m. Sedimentation rates tested ranged from 1 to 30 cm/kyr with a step of 0.2 cm/kyr.

where x refers to the orbitally tuned stratigraphic proxy series. The ρ_1 model is advantageous because it is not affected by band selection and can be used to directly evaluate the time series. The ρ_1 approach has been applied as a noise-independent indicator of changes in relative sea or lake level. Lower noise is associated with higher ρ_1 values, while higher

noise leads to a reduction in ρ_1 (Li et al., 2018a; Wang et al., 2020).

4 Results

4.1 Cycles in the stratigraphic domain

The MTM analyses of untuned GR series in well MY-1 reveal remarkably robust peaks at 37, 16.5, 8.5, 4.4, 3.6, 2.8, 2.1, and 1.2–1.32 m with confidence levels of astronomical forcing exceeding 95%. The 50, 12.6, 8.4, 4.7, 3.3–3, 2.4, and 1.9 m wavelengths were all above 95% confidence in the XY-1 borehole; the 28.4, 9.7, 5.9–5.6, 2.3–1.9, and 1.4 m wavelengths were above 95% confidence in the X-203 borehole; and the 42.8, 13.9, 11, 5.1, 3.7, 3, 2.4, and 1.8–1.6 m wavelengths also indicate high confidence levels in the M-49 borehole (Figure 3).

The COCO algorithm, which is designed for verifying optimal sedimentation rates, was conducted for 2,000 Monte Carlo simulations to ensure the accuracy of the results. Synthesis of the eCOCO analysis technique, which calculates the estimations of sedimentations with ranges consistent with those derived from the COCO method, allows the favorable geological constraint for local sedimentation rates to be determined. Using null hypothesis significance levels < 0.01, the most prominent peaks occurring at 9.3 and 17 cm/kyr represent the most likely sedimentation rates in MY-1 well (Figure 4A). Previous cyclostratigraphic analyses using density logging data indicated that the average deposition rate of the P_1f_1 and P_1f_2 members of the Fengcheng Formation was approximately 9 cm/kyr (e.g., Tang et al., 2022). We therefore preferred the 9.3 cm/kyr peak as the optimal rate of sedimentation. In this case, the 37-m wavelength in well MY-1 tended toward the long eccentricity cycle. Similarly, the COCO and eCOCO results indicate optimal rates of sedimentation in wells XY-1, X-203, and M-49 of 13.5–14.5, 7.2, and 13.8 cm/kyr, respectively (Figures 4B–D). The peaks at 50 m in well XY-1, 28.4 m in well X-203, and 42.8 m in well M-49 therefore all indicate long eccentricity cycles (405 kyr). The sedimentation rate variations in the depth domain are illustrated by the evolutionary FFT spectrograms, which show stabilized ~40–50-m-long eccentricity cycles throughout the entire succession (Figure 3). Long eccentricity cycles within the GR series were separated using Gaussian bandpass filtering (Kodama and Hinnov, 2014).

Stratigraphic correlation of the Mahu Sag reveals that the deposition of the Fengcheng Formation occurred at approximately 300 Ma, developing mainly in the Asselian stage of the Early Permian (Cao et al., 2020; Huang et al., 2021; Tang et al., 2022). In addition to stable long eccentricity, the precession and obliquity cycles also exhibited shorter periods (Berger et al., 1992; Laskar et al., 2004; Waltham, 2015). Following Berger et al. (1992), the obliquity period during the Fengcheng Formation's sedimentary stage is 34.2 kyr, and the precession periods are 20.7 and 17.4 kyr, all of which contain values obtained from the "Milankovitch calculator" of Waltham (2015) and associated errors (35.5 ± 2.9 kyr for obliquity and 21.7 ± 1.1 kyr to 17.66 ± 0.76 kyr for the precession components). This study selected orbital parameter periods of 405, 100, and 34.2 kyr for long (E) and short eccentricities (e) and obliquity (O), respectively, and 20.7 and 17.4 kyr for precession (P). These interpreted orbital cycle wavelengths of 28.4–50, 5.9–12.6, 2.3–3.9, and 1.2–2.7 m are listed in Table 1. The ratio relationship between these wavelengths is very consistent with the theoretical astronomical period ratio in the Early Permian (Berger et al., 1992; Waltham, 2015).

4.2 Cycles in the time domain

We tuned the assumed stratigraphic cycles to astronomical frequencies in the time domain to eliminate the effect of sedimentation rate variations. The preferred method for tuning (depth to time) individual stratigraphic spectral peaks to a defined target astronomical frequency is minimal tuning, thereby aligning certain stratigraphic spectral peaks to other astronomical frequencies. The long eccentricity cycle is theoretically influenced by the orbital perihelia of Jupiter and Venus. Jupiter's large mass ensures that this cycle is robustly modeled over several hundreds of Myr (Berger et al., 1992; Laskar et al., 2004; Hinnov, 2013). The long eccentricity cycle therefore serves essentially as a "metronome" in astrochronology and has accordingly been applied for calibrating the geological time scale (e.g., Hinnov and Hilgen, 2012; Wang et al., 2020; Liu et al., 2022; Wei et al., 2023). Tuning the approximately 40–50 m cycles of the time series to the long eccentricity cycle enables the number of eccentricity cycles to be recognized. Following the theoretically optimal rates of sedimentation mapped in the COCO/eCOCO spectrograms (Figure 4), we applied a Gaussian bandpass filter to extract the ~37-m cycle band from the MY-1 series, the ~50-m cycle band from the XY-1 series, the ~28.4-m from the X-203 series, and the ~42.8-m from the M-49 series, each with a bandwidth of 40%.

Figure 5 shows significant peaks (> 90%–99% confidence) in the MTM power spectra of the 405-kyr-tuned GR series from the four boreholes, which agrees well with the theoretically predicted periodicities of E, e, O, and P during the Early Permian (Berger et al., 1992; Waltham, 2015). The floating ATS for wells MY-1, XY-1, X-203, and M-49 were accordingly established as ~3.8, ~4.48, ~5.18, and ~4.7 Myr, respectively. The high-resolution ATS is an important guideline for dividing the high-frequency sedimentary framework and correlating the four wells. As mentioned, the Fengcheng Formation's P_1f_1 and P_1f_2 members are the primary focus of our cyclostratigraphic analyses. Stratigraphic correlations based on the long eccentricity cycle show that the P_1f_2 and P_1f_3 member durations are ~2.4 and ~1.2 Myr (Figure 6). We have therefore established a convincing framework of the four single wells, as well as a contemporaneous stratigraphic correlation scheme for the section along the provenance direction in the context of astronomical chronology. However, the possibility of establishing an absolute time scale for the P_1f_1 and P_1f_2 members is limited, partly owing to the deficiency of an absolute age anchor for the floating ATS.

TABLE 1 Power peaks of the GR series from the Fengcheng Formation.

Borehole	Thickness (m)	Interpreted orbital cycle (m)					Ratio
		E	e	O	P1	P2	E: e: O: P1: P2
MY-1	439.9	37	8.5	2.8	1.32	1.2	30.8:7.08:2.3:1.1:1
XY-1	555	50	12.6	3.9	2.72	2.4	20.8:5.3:1.6:1.13:1
X-203	358	28.4	5.9	2.3	1.7	1.4	20.3:4.2:1.6:1.2:1
M-49	397.76	42.8	11	3.7	1.8	1.6	26:6.9:2.3:1.1:1

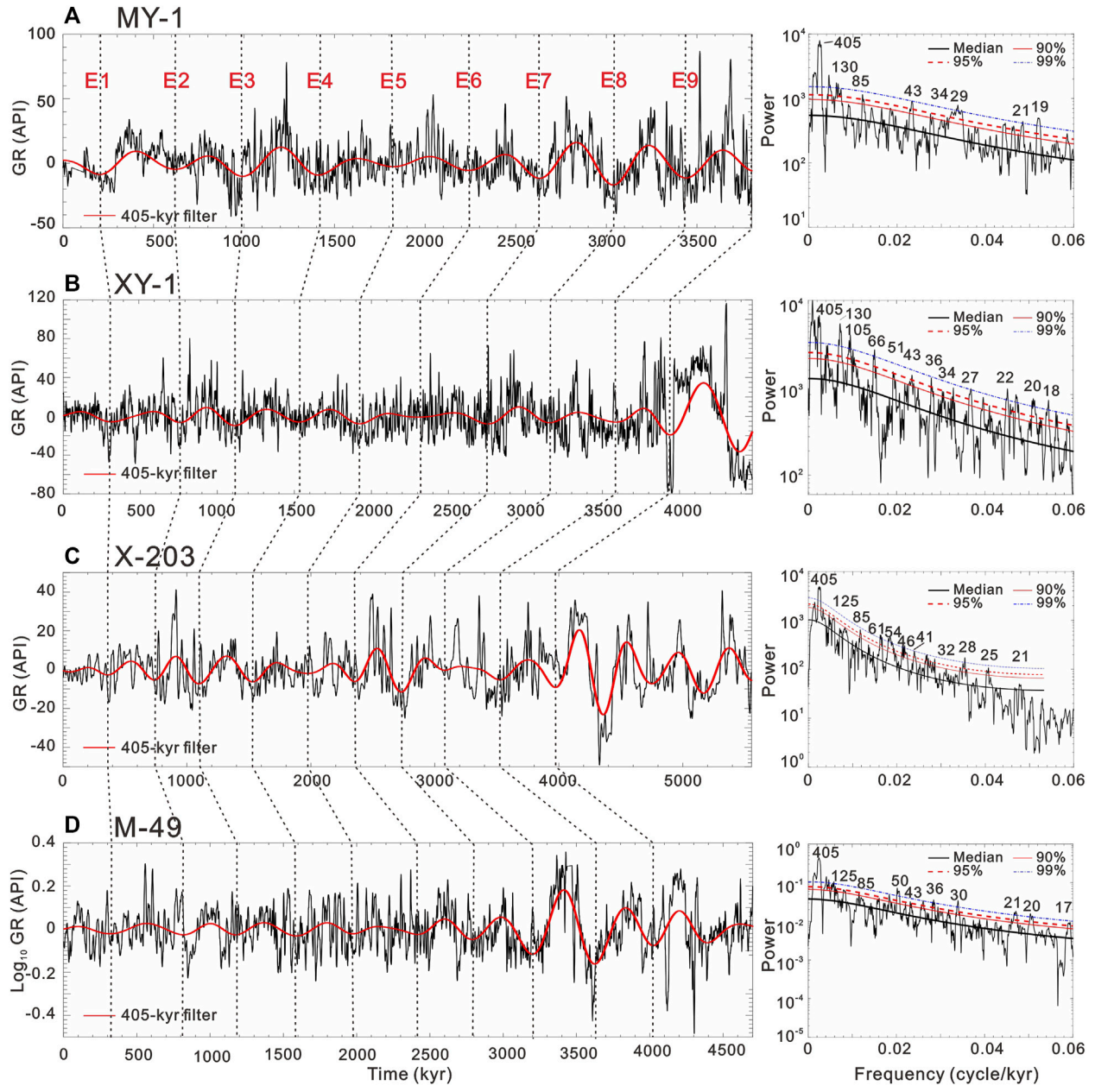

FIGURE 5
Spectral analyses of GR series from wells MY-1 **(A)**, XY-1 **(B)**, X-203 **(C)**, and M-49 **(D)** after tuning to the time domain. Also shown are the detrended GR series (black curve) and filtered long eccentricity cycles (red curve, 405 kyr) with passbands of 0.00246 ± 0.0005 cycle/kyr, and the 2π MTM analysis results of the tuned GR time series, with significant peaks labeled in units of kyr.

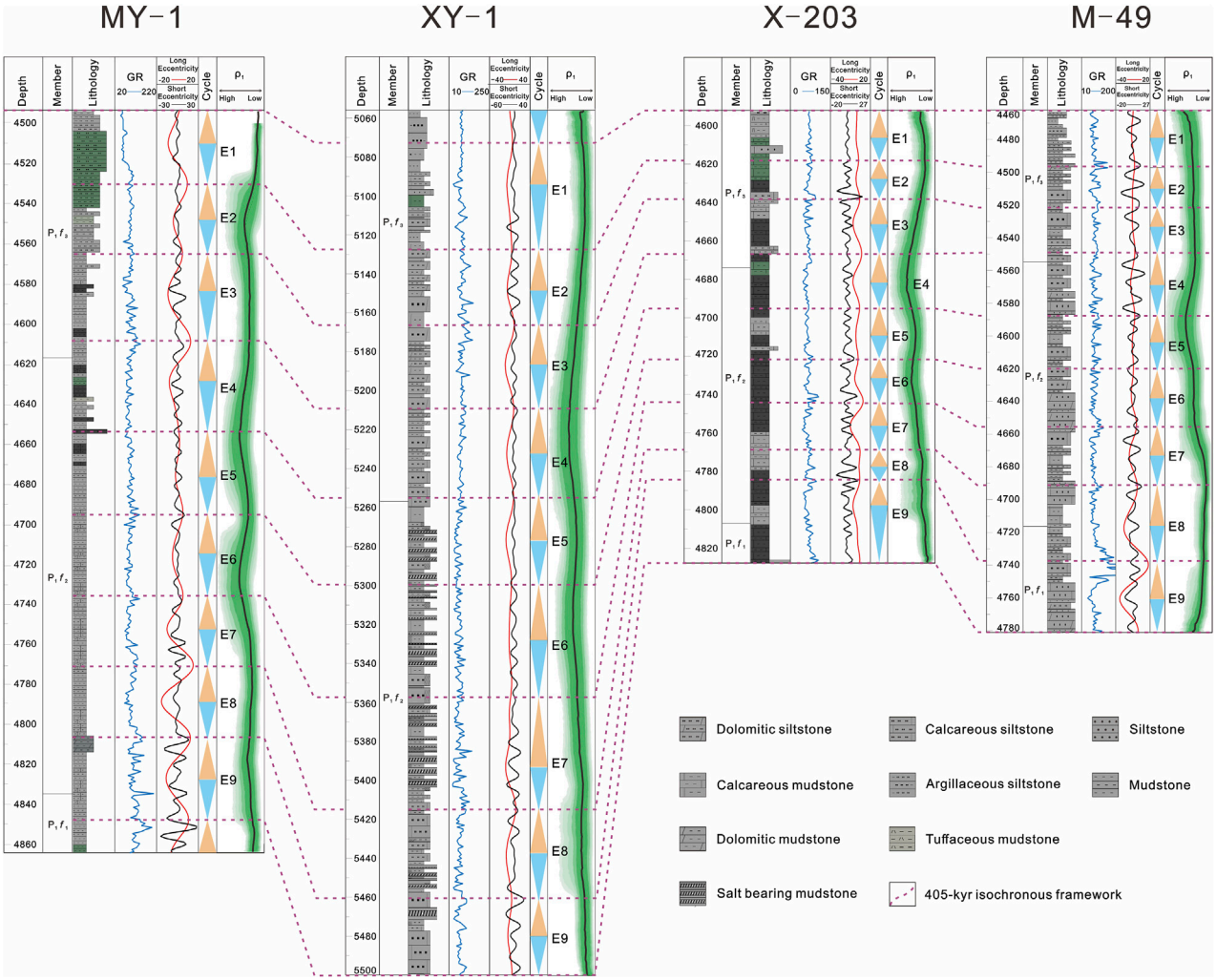

FIGURE 6
High-frequency isochronous sedimentary framework division and correlation and lake-level changes of the Fengcheng Formation in the Mahu Sag. The dashed purple line represents the boundary of 405 kyr long eccentricity cycles. The ρ_1 models of the tuned GR series were estimated using a running window of 405 kyr. A Monte Carlo analysis with 2,000 iterations was performed to estimate the confidence level.

5 Discussion

5.1 High-frequency sedimentary framework division and correlation

The sedimentary sequence hierarchy is based mostly on the timing and amplitude of sea level oscillations (e.g., Vail et al., 1977; Boulila et al., 2011). Recent reports have argued that climate change associated with orbital forcing is the major factor that controls the development of third-order and higher frequency sequences (Boulila et al., 2011; Liu et al., 2022; Wu et al., 2022). The third-order sequences may be connected to ~2.4 Myr long-period eccentricity and ~1.2 Myr long-period obliquity (e.g., Boulila et al., 2011; Cong et al., 2019; Du et al., 2020). Notably, this hierarchy can account for orbital frequency evolution throughout geological time. For example, the ~1.2- and ~2.4-Myr cycles may have undergone variations owing to the inner planets' chaotic motion (Laskar, 1989; Laskar et al., 2004). Previous theoretical work (DeConto and Pollard, 2003) suggested that glacioeustatic falls owing to orbital forcing are connected with the 405-kyr and ~2.4-Myr eccentricity minima. Fourth-order and well-documented stratigraphic sequences (Boulila et al., 2010; Boulila et al., 2011) may be reflective of the 405-kyr eccentricity cycle (Laskar et al., 2004), which is astronomically stable, and potentially the ~160–200-kyr short obliquity modulations. The fifth-order sequences may be related to the short eccentricity cycle, while sixth-order sequences could be connected to fundamental cycles of precession (~20 kyr) and/or obliquity (~40 kyr) (Boulila et al., 2010; Boulila et al., 2011). The obliquity precession components were also shorter within deep time owing to tidal dissipation (Berger et al., 1992; Laskar et al., 2004; Waltham, 2015). The simple connection between eustatic and astronomical hierarchies does not eliminate numerous stochastic feedbacks and processes that interfere with changes in sea level and climate, such as greenhouse gas effects, tectonics, and intrinsic ice dynamics.

For lacustrine shales, the climate change caused by the orbital cycle controls the development of third-to sixth-order high-frequency sequences. The third-order sequence is a lake transgression-regression sequence with large-scale lake-level changes comparable to long-term base-level cycles, and is controlled by the ~2.4 Myr long-period eccentricity and ~1.2 Myr long-period obliquity cycle (Boulila et al., 2011; Wang et al., 2020; Wei et al., 2023). The fourth-order sequence is a secondary lake transgression-regression sequence with high-amplitude water depth changes corresponding to the medium-term base-level cycle and controlled by the 405 kyr long eccentricity cycle (Boulila et al., 2011; Liu et al., 2022). The fifth-order sequence is a rhythmic transgression-regression sequence with low amplitude lake-level change corresponding to the short-term base-level cycle and controlled by the ~100 kyr short eccentricity cycle (Boulila et al., 2010; Boulila et al., 2011; Tang et al., 2022). Many scholars therefore use different orders of eccentricity cycles as a reference to divide the high-frequency cycle framework of lacustrine shale sequences (e.g., Cong et al., 2019; Du et al., 2020; Fang et al., 2023).

Cyclostratigraphic analyses of four standard wells were conducted in this study to establish an isochronous cycle framework for the Fengcheng Formation (Figure 6). Using the 405-kyr eccentricity cycle as a reference, nine medium-term base-level cycles (E1–E9) were identified within the P_1f_1 and P_1f_2 members that roughly correspond to fourth-order sequences. Each long eccentricity cycle consists of approximately four ~100-kyr short eccentricity cycles, which allows approximately 36 short-term base-level cycles to be identified, roughly corresponding to fifth-order sequences.

Under the constraints of isochronous stratigraphic framework, the Fengcheng Formation's sedimentation rate is positively correlated with the depositional thickness. During the Fengcheng Formation's depositional period, the Zaire and Haraalat Mountains, which are found on the western margin of the Junggar Basin, provided the major terrigenous supply (Song et al., 2022). The Fengcheng Formation on the northwestern margin of the Mahu Sag inherited and then developed a multisource fan delta sedimentary system. The sedimentation rate of well M-49 (13.8 cm/kyr) is higher than that of both wells MY-1 (9.3 cm/kyr) and X-203 (7.2 cm/kyr), likely because its location received more terrigenous clastic material supply. The sedimentation rate of well XY-1 (13.5 cm/kyr) is also relatively high owing to the large and rapid accumulation of alkaline minerals.

The application of astronomical cycles to stratigraphic sequences enables high-resolution isochronous stratigraphic correlation at the eccentricity cycle scale, thus overcoming the long-standing bottleneck of low precision when using traditional methods for the subdivision and correlation of deep-water shale sequences. This novel approach shows great potential for fine-scale characterization of alkaline lacustrine sequences and provides innovative insights for predicting favorable areas for shale oil exploration.

5.2 Astronomical forcing of paleolake-level variations

Sedimentary noise model involves two complementary approaches: the dynamic noise after orbital tuning (DYNOT) model and Lag-1 autocorrelation coefficient (ρ_1) model (Li et al., 2018a). While the former is typically used to examine temporal shifts in lake level, the latter is commonly used to analyze changes in lake level with respect to stratigraphic depth. The primary goal of our research is to use astronomical cycles to constrain the stratigraphic framework, focusing primarily on the ρ_1 model to reconstruct lake-level variations in the depth domain. Continental basins are sensitive to climate changes and have high sedimentation rates and high sedimentary record temporal resolutions, which can record long-term paleoclimate signals. This model has been applied in studies of lake-level changes during multiple geological epochs. Increasing evidence suggests the applicability of the sedimentary noise model (e.g., Wang et al., 2020; Huang et al., 2021; Tang et al., 2022; Wei et al., 2023). Compared with traditional methods, this approach is characterized by the direct quantitative evaluation of sedimentary noise using paleoclimate proxies in the depth domain. Compared with traditional reconstruction methods, such as sequence stratigraphy, the results are objective and independent of researcher experience.

The ρ_1 model using a tuned GR series with a 400-kyr sliding window allows the autocorrelation curve of the Fengcheng Formation to be reconstructed. Following our hypothesis in Section 3.3, we propose that the curve is representative of the relative water level variation in the paleolake. In this study, lake-level variations in the Mahu Sag exhibit significant periodicity. In particular, ρ_1 of the middle part of the Fengcheng Formation (P_1f_2 Member) is larger and shows a relatively higher lake level (Figure 6). This study identified nine mid-term base-level cycles (E1–E9) within the P_1f_1 and P_1f_2 members, each lasting approximately 405 kyr. The lake-level rise was particularly significant during cycles E9, E6, E5, and E4. The E9 cycle corresponds to the late depositional stage of the P_1f_1 Member, with a relatively low input of terrestrial debris and thin deposits of organic-rich mudstones in the Mahu Sag, indicating a reducing environment. During the early depositional stage of the P_1f_2 Member, the basin decreased in size and the regional climate became arid. The input of terrigenous debris remains relatively low, resulting in an increase in lake salinity and water stratification. Cycles E6 to E4 correspond to the middle to late stages of P_1f_2 Member deposition, during which time the basin expanded again. The climate at this time was extremely hot and dry, and the lake water salinity reached its highest level. Alkaline minerals were widely developed, and even deposits of reedmergnerite occurred (Zhang et al., 2018; Song et al., 2022). During the deposition of the P_1f_3 Member, the basin further contracted, and the salinity gradually decreased as the lake level proceeded to drop. The climate then became more humid and warmer, and the terrestrial debris input increased, but the organic matter abundance decreased. The basin developed toward freshening, characterized by an increase in the input of terrigenous clastic sediments.

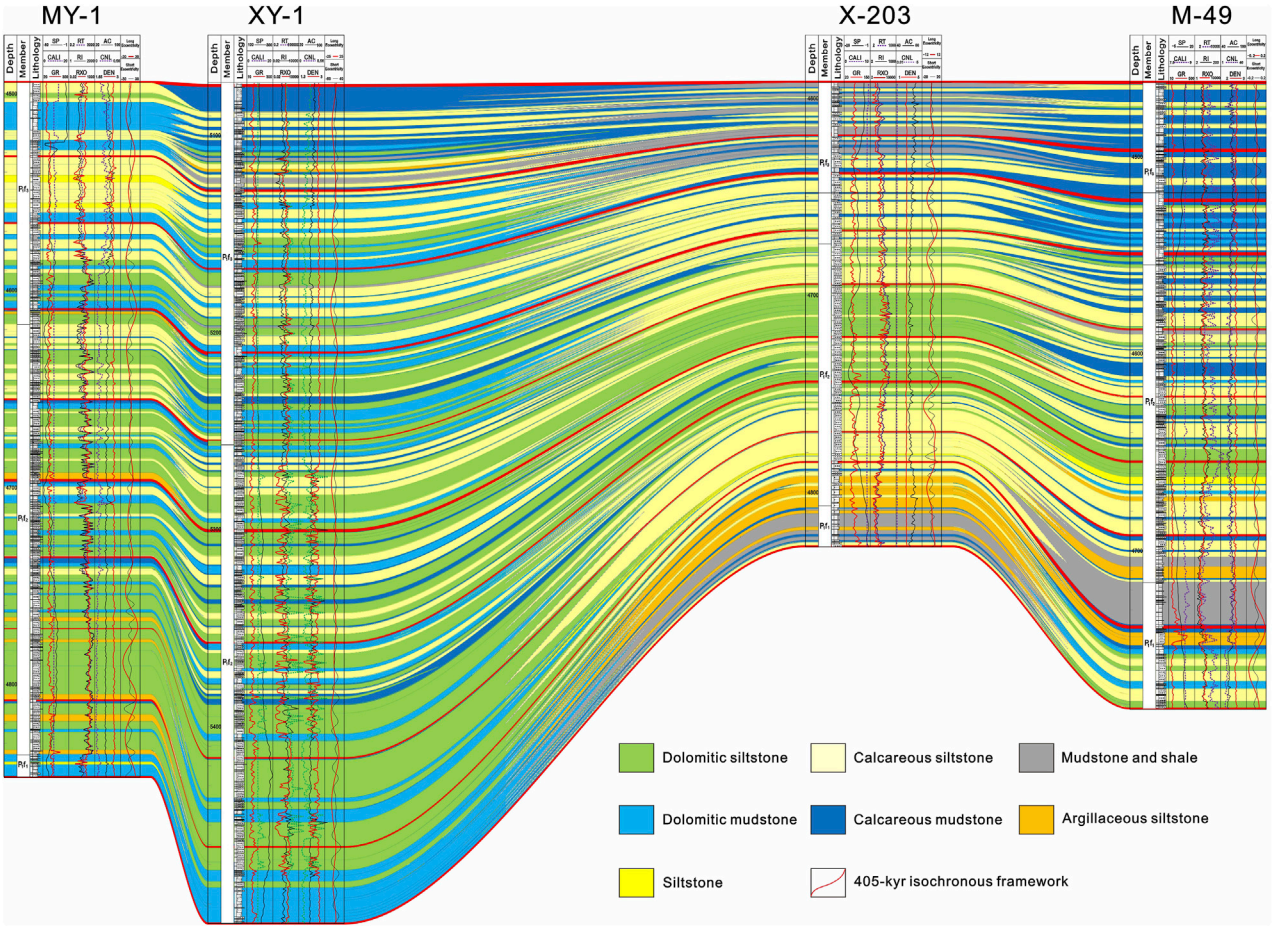

FIGURE 7
Lithofacies distribution of the Fengcheng Formation based on the high-frequency sedimentary framework in the Mahu Sag. Combined with the indicative significance of various conventional logging curves for lithofacies, the lithofacies types of the Fengcheng Formation were classified into dolomitic siltstone, dolomitic mudstone, calcareous siltstone, calcareous mudstone, mudstone and shale, argillaceous siltstone, siltstone, and other types. The red line represents the boundary of 405 kyr long eccentricity cycles. Correlation of lithofacies distribution was performed under the constraints of long eccentricity cycles.

5.3 Lithofacies distribution in the high-frequency sedimentary framework

Earth's orbital cycles can modulate the sedimentary processes and depositional environments of lacustrine shales, leading to the formation of distinct lithofacies patterns. The resulting lithofacies can reveal information about the paleoenvironmental conditions, such as climate and lake-level fluctuations, that prevailed during the deposition of the shale sequence. Regulated by changes in lake level and high-frequency cycles, the Fengcheng Formation in the Mahu Sag comprises a diverse array of sedimentary rocks, including terrestrial fan-delta clastic rocks, endogenic carbonate rocks, volcaniclastic rocks, evaporites, and mixed sedimentary rocks (Yu et al., 2018a; Zhang et al., 2018; Song et al., 2022). Further combining the significance of a variety of conventional logging curves to indicate the lithology, we classify the lithofacies types of the Fengcheng Formation into dolomitic siltstone, dolomitic mudstone, calcareous siltstone, calcareous mudstone, mudstone and shale, argillaceous siltstone, siltstone and others (Figure 7).

Isochronous stratigraphic correlation was conducted along the provenance direction in the northern area of the Mahu Sag, which reveals the presence of at least 36 short-term base-level cycles within the P_1f_1 and P_1f_2 members, with a lithofacies identification resolution reaching the level of short eccentricity (~100 kyr) (Figure 7). The spatial distribution patterns of lithofacies in the Fengcheng Formation can be clearly demonstrated within the isochronous cycle framework under the 405-kyr long eccentricity cycle constraints. Alkaline mineral lithofacies dominate in the P_1f_2 Member, while organic-rich shale lithofacies are prevalent in the upper section of the P_1f_1 Member and the lower part of the P_1f_3 Member, which are often interbedded with limestone lithofacies.

Wells MY-1 and XY-1 are located closer to the lake sedimentary center, where the thickness of evaporite deposition is greater. The duration of the P_1f_1 Member represents the early stage of alkaline lake evolution, characterized by dolomitic mudstone and calcareous mudstone lithofacies. The duration of the P_1f_2 Member is marked by the intensive deposition of alkaline minerals and the development of dolomitic mudstone and dolomite lithofacies. The duration of the P_1f_3 Member represents the extinction stage of the alkaline lake, with

dolomitic siltstone and calcareous mudstone lithofacies developed in this area. In contrast, the depositional thickness of evaporites near the slope edge of the lake (Wells X-203 and M-49) is small, and the lithofacies is characterized by calcareous siltstone and coarse clastic sediments.

Future work will involve the identification of high-frequency cycles that are enriched in shale oil, followed by the detailed characterization of the lithofacies within these cycles, to reveal the sedimentary response of organic-rich shale deposition to astronomical orbital forcing.

6 Conclusion

Cyclostratigraphic analyses in wells MY-1, XY-1, X-203, and M-49 allowed the identification that the Fengcheng Formation exhibits significant astronomical cycles, including the 405-kyr long eccentricity cycle, the ~100-kyr short eccentricity cycle, and the obliquity and precession cycle. These results show that the sedimentation process in the alkaline lacustrine areas of the Fengcheng Formation was astronomically controlled. Stratigraphic correlations based on the long eccentricity cycle show that the duration of the P_1f_2 Member is ~2.4 Myr and that of the P_1f_3 Member is ~1.2 Myr.

There is a strong correlation between Earth's orbital cycles and sedimentary sequences in the Fengcheng Formation. Nine medium-term base-level cycles (E1–E9) were identified within the P_1f_1 and P_1f_2 members, which roughly correspond to fourth-order sequences. These cycles are approximately 405 kyr and consist of approximately four ~100 kyr short eccentricity cycles, resulting in the identification of approximately 36 short-term base-level cycles, generally corresponding to fifth-order sequences. The sedimentary noise modeling method was applied to reconstruct paleolake-level variations in the Fengcheng Formation. The results revealed that the lake level significantly increased during the E9, E6, E5, and E4 cycles. The Fengcheng Formation exhibits clear spatial distribution patterns of lithofacies within the isochronous cycle framework. Future work will involve the identification of shale oil-enriched cycles and investigation of astronomical cycle control over organic matter enrichment.

Data availability statement

The original contributions presented in the study are included in the article/Supplementary Material, further inquiries can be directed to the corresponding author.

Author contributions

Conceptualization and investigation: GL, RZ, and RkZ; methodology: XH and RWe; formal analysis: WH, MZ, QC, RWa, and XZ; writing–original draft: GL, RZ, XH, and RWe; review and editing: RZ, RkZ, and YT. All authors contributed to the article and approved the submitted version.

Funding

This work was financially supported by the National Natural Science Foundation of China (Grant Nos 42090025, 42102166).

Acknowledgments

We would like to thank the editors and reviewers whose input greatly improved the quality of this manuscript.

Conflict of interest

Authors GL, RkZ, YT, WH, MZ, QC, RWa, and XZ were employed by the company PetroChina.

The remaining authors declare that the research was conducted in the absence of any commercial or financial relationships that could be construed as a potential conflict of interest.

Publisher's note

Supplementary material

The Supplementary Material for this article can be found online at: https://www.frontiersin.org/articles/10.3389/feart.2023.1206835/full#supplementary-material

References

Anderson, R. (1982). A long geo-climatic record from the Permian. *J. Geophys. Res.* 87, 7285–7294. doi:10.1029/JC087iC09p07285

Berger, A., Loutre, M., and Laskar, J. (1992). Stability of the astronomical frequencies over the Earth's history for paleoclimate studies. *Science* 255, 560–566. doi:10.1126/science.255.5044.560

Boulila, S., Galbrun, B., Hinnov, L. A., Collin, P.-Y., Ogg, J. G., Fortwengler, D., et al. (2010). Milankovitch and sub-milankovitch forcing of the oxfordian (late jurassic) terres noires formation (SE France) and global implications. *Basin Res.* 22, 717–732. doi:10.1111/j.1365-2117.2009.00429.x

Boulila, S., Galbrun, B., Miller, K. G., Pekar, S. F., Browning, J. V., Laskar, J., et al. (2011). On the origin of Cenozoic and Mesozoic "third-order" eustatic sequences. *Earth-Sci. Rev.* 109, 94–112. doi:10.1016/j.earscirev.2011.09.003

Cao, J., Xia, L., Wang, T., Zhi, D., Tang, Y., and Li, W. (2020). An alkaline lake in the late paleozoic ice age (lpia): A review and new insights into paleoenvironment and petroleum geology. *Earth-Sci. Rev.* 202, 103091. doi:10.1016/j.earscirev.2020.103091

Cleveland, W. S. (1979). Robust locally weighted regression and smoothing scatterplots. *Publ. Am. Stat. Assoc.* 74, 829–836. doi:10.1080/01621459.1979.10481038

Cong, F., Zhu, F., Cai, Z., Chen, H., Li, J., Wang, Y., et al. (2019). Orbitally forced glacio-eustatic origin of third-order sequences and parasequences in the Middle Permian Maokou Formation, South China. *Mar. Pet. Geol.* 99, 237–251. doi:10.1016/j.marpetgeo.2018.10.014

DeConto, R., and Pollard, D. (2003). Rapid Cenozoic glaciation of Antarctica induced by declining atmospheric CO_2. *Nature* 421, 245–249. doi:10.1038/nature01290

Du, W., Ji, Y., Chen, G., Wu, H., Gao, C., Li, S., et al. (2020). Cyclostratigraphy and astronomical tuning during the oligocene in the jizhong depression, bohai bay basin,

northeastern China. *Palaeogeogr. Palaeoclimatol. Palaeoecol.* 554, 109803. doi:10.1016/j.palaeo.2020.109803

Eldrett, J. S., Ma, C., Bergman, S. C., Ozkan, A., Minisini, D., Lutz, B., et al. (2015). Origin of limestone–marlstone cycles: Astronomic forcing of organic-rich sedimentary rocks from the Cenomanian to early Coniacian of the Cretaceous Western Interior Seaway, USA. *Earth Planet. Sci. Lett.* 423, 98–113. doi:10.1016/j.epsl.2015.04.026

Fang, Z., Zhang, L., and Ma, C. (2023). Development and controlling factors of shale lithofacies cycles in a continental rift basin: A case study of Es_4^u in the boxing subsag of dongying sag, bohai bay basin, China. *Front. Earth Sci.* 11, 1136012. doi:10.3389/feart.2023.1136012

Hinnov, L. A. (2013). Cyclostratigraphy and its revolutionizing applications in the Earth and planetary sciences. *Geol. Soc. Am. Bull.* 125, 1703–1734. doi:10.1130/B30934.1

Hinnov, L. A., and Hilgen, F. J. (2012). "Chapter 4 - cyclostratigraphy and astrochronology," in *The geologic time scale*. Editors F. M. Gradstein, J. G. Ogg, M. D. Schmitz, and G. M. Ogg (Boston: Elsevier), 63–83. doi:10.1016/B978-0-444-59425-9.00004-4

Huang, C., and Hinnov, L. (2019). Astronomically forced climate evolution in a saline lake record of the middle Eocene to Oligocene, Jianghan Basin, China. *Earth Planet. Sci. Lett.* 528, 115846. doi:10.1016/j.epsl.2019.115846

Huang, H., Gao, Y., Jones, M. M., Tao, H., Carroll, A. R., Ibarra, D. E., et al. (2020). Astronomical forcing of Middle Permian terrestrial climate recorded in a large paleolake in northwestern China. *Palaeogeogr. Palaeoclimatol. Palaeoecol.* 550, 109735. doi:10.1016/j.palaeo.2020.109735

Huang, H., Gao, Y., Ma, C., Niu, L., Dong, T., Tian, X., et al. (2021). Astronomical constraints on the development of alkaline lake during the carboniferous-permian period in north pangea. *Glob. Planet. Change* 207, 103681. doi:10.1016/j.gloplacha.2021.103681

Kent, D. V., Olsen, P. E., and Muttoni, G. (2017). Astrochronostratigraphic polarity time scale (APTS) for the Late Triassic and Early Jurassic from continental sediments and correlation with standard marine stages. *Earth-Sci. Rev.* 166, 153–180. doi:10.1016/j.earscirev.2016.12.014

Kodama, K. P., and Hinnov, L. A. (2014). *Rock magnetic cyclostratigraphy*. United States: Wiley. doi:10.1002/9781118561294

Kuang, L., Tang, Y., Lei, D., Chang, Q., Ouyang, M., Hou, L., et al. (2012). Formation conditions and exploration potential of tight oil in the Permian saline lacustrine dolomitic rock, Junggar Basin, NW China. *Pet. Explor. Dev.* 39, 700–711. doi:10.1016/S1876-3804(12)60095-0

Laskar, J. (1989). A numerical experiment on the chaotic behaviour of the Solar System. *Nature* 338, 237–238. doi:10.1038/338237a0

Laskar, J., Robutel, P., Joutel, F., Gastineau, M., Correia, A. C. M., and Levrard, B. (2004). A long-term numerical solution for the insolation quantities of the Earth. *Astron. Astrophys.* 428, 261–285. doi:10.1051/0004-6361:20041335

Li, M., Hinnov, L. A., Huang, C., and Ogg, J. G. (2018a). Sedimentary noise and sea levels linked to land–ocean water exchange and obliquity forcing. *Nat. Commun.* 9, 1004. doi:10.1038/s41467-018-03454-y

Li, M., Hinnov, L., and Kump, L. (2019a). Acycle: Time-series analysis software for paleoclimate research and education. *Comput. Geosci.* 127, 12–22. doi:10.1016/j.cageo.2019.02.011

Li, M., Huang, C., Ogg, J., Zhang, Y., Hinnov, L., Wu, H., et al. (2019b). Paleoclimate proxies for cyclostratigraphy: Comparative analysis using a Lower Triassic marine section in South China. *Earth-Sci. Rev.* 189, 125–146. doi:10.1016/j.earscirev.2019.01.011

Li, M., Kump, L. R., Hinnov, L. A., and Mann, M. E. (2018b). Tracking variable sedimentation rates and astronomical forcing in Phanerozoic paleoclimate proxy series with evolutionary correlation coefficients and hypothesis testing. *Earth Planet. Sci. Lett.* 501, 165–179. doi:10.1016/j.epsl.2018.08.041

Liu, S., Jin, S., Liu, Y., and Chen, A. (2022). Astronomical forced sequence infill of early cambrian Qiongzhusi organic-rich shale of Sichuan Basin, south China. *Sediment. Geol.* 440, 106261. doi:10.1016/j.sedgeo.2022.106261

Mann, M. E., and Lees, J. M. (1996). Robust estimation of background noise and signal detection in climatic time series. *Clim. Change* 33, 409–445. doi:10.1007/BF00142586

Meyers, S. R. (2019). Cyclostratigraphy and the problem of astrochronologic testing. *Earth-Sci. Rev.* 190, 190–223. doi:10.1016/j.earscirev.2018.11.015

Meyers, S. R., and Hinnov, L. A. (2010). Northern Hemisphere glaciation and the evolution of Plio-Pleistocene climate noise. *Paleoceanography* 25. doi:10.1029/2009PA001834

Mudelsee, M. (2002). Tauest: A computer program for estimating persistence in unevenly spaced weather/climate time series. *Comput. Geosci.* 28, 69–72. doi:10.1016/S0098-3004(01)00041-3

Olsen, P., and Kent, D. (1996). Milankovitch climate forcing in the tropics of pangaea during the late triassic. *Palaeogeogr. Palaeoclimatol. Palaeoecol.* 122, 1–26. doi:10.1016/0031-0182(95)00171-9

Song, Y., Yang, Z., He, W., Gan, R., Zhang, R., Huang, L., et al. (2022). Exploration progress of alkaline lake type shale oil of the permian Fengcheng Formation in Mahu sag, Junggar Basin. *China Pet. explor.* 27, 60–72.

Tang, Y., Zheng, M., Wang, X., Wang, T., Cheng, H., and Hei, C. (2022). The floating astronomical time scale for the terrestrial Early Permian Fengcheng Formation from the Junggar Basin and its stratigraphic and palaeoclimate implications. *Geol. J.* 57, 4842–4856. doi:10.1002/gj.4575

Thomson, D. J. (1982). Spectrum estimation and harmonic analysis. *Proc. IEEE* 70, 1055–1096. doi:10.1109/PROC.1982.12433

Vail, P. R., Mitchum, R. M., Todd, J. R. G., Widmier, J. M., Thompson, S., Sangree, J. B., et al. (1977). Seismic stratigraphy and global changes of sea level: Seismic stratigraphy – applications to hydrocarbon exploration. *Mem. Am. Ass. Pertol. Geol.* 26, 49–212.

van Vugt, N., Langereis, C. G., and Hilgen, F. J. (2001). Orbital forcing in pliocene–pleistocene mediterranean lacustrine deposits: Dominant expression of eccentricity versus precession. *Palaeogeogr. Palaeoclimatol. Palaeoecol.* 172, 193–205. doi:10.1016/S0031-0182(01)00270-X

Waltham, D. (2015). Milankovitch period uncertainties and their impact on cyclostratigraphy. *J. Sediment. Res.* 85, 990–998. doi:10.2110/jsr.2015.66

Wang, M., Chen, H., Huang, C., Kemp, D. B., Xu, T., Zhang, H., et al. (2020). Astronomical forcing and sedimentary noise modeling of lake-level changes in the Paleogene Dongpu Depression of North China. *Earth Planet. Sci. Lett.* 535, 116116. doi:10.1016/j.epsl.2020.116116

Wang, T., Cao, J., Carroll, A. R., Zhi, D., Tang, Y., Wang, X., et al. (2021). Oldest preserved sodium carbonate evaporite: Late paleozoic Fengcheng Formation, Junggar Basin, NW China. *GSA Bull.* 133, 1465–1482. doi:10.1130/B35727.1

Wang, X., Jin, Z., Chen, G., Peng, M., Huang, L., Wang, Z., et al. (2022). Multi-scale natural fracture prediction in continental shale oil reservoirs: A case study of the Fengcheng Formation in the Mahu sag, Junggar Basin, China. *Front. Earth Sci.* 10, 929467. doi:10.3389/feart.2022.929467

Weedon, G. P. (2003). *Time series analysis and cyclostratigraphy: Examining stratigraphic records of environmental cycles*. Cambridge, United Kingdom: Cambridge University Press.

Wei, R., Zhang, R., Li, M., Wang, X., and Jin, Z. (2023). Obliquity forcing of lake-level changes and organic carbon burial during the Late Paleozoic Ice Age. *Glob. Planet. Change* 223, 104092. doi:10.1016/j.gloplacha.2023.104092

Wu, H., Hinnov, L. A., Zhang, S., Jiang, G., Yang, T., Li, H., et al. (2022). Continental geological evidence for solar system chaotic behavior in the late cretaceous. *GSA Bull.* 135, 712–724. doi:10.1130/B36340.1

Wu, H., Zhang, S., Jiang, G., Hinnov, L., Yang, T., Li, H., et al. (2013). Astrochronology of the early turonian–early campanian terrestrial succession in the songliao basin, northeastern China and its implication for long-period behavior of the solar system. *Palaeogeogr. Palaeoclimatol. Palaeoecol.* 385, 55–70. doi:10.1016/j.palaeo.2012.09.004

Yu, K., Cao, Y., Qiu, L., Sun, P., Jia, X., and Wan, M. (2018b). Geochemical characteristics and origin of sodium carbonates in a closed alkaline basin: The lower permian Fengcheng Formation in the Mahu sag, northwestern Junggar Basin, China. *Palaeogeogr. Palaeoclimatol. Palaeoecol.* 511, 506–531. doi:10.1016/j.palaeo.2018.09.015

Yu, K., Cao, Y., Qiu, L., and Sun, P. (2018a). The hydrocarbon generation potential and migration in an alkaline evaporite basin: The Early Permian Fengcheng Formation in the Junggar Basin, northwestern China. *Mar. Pet. Geol.* 98, 12–32. doi:10.1016/j.marpetgeo.2018.08.010

Zhang, R., Jin, Z., Liu, Q., Li, P., Huang, Z., Shi, J., et al. (2019). Astronomical constraints on deposition of the middle triassic chang 7 lacustrine shales in the ordos basin, central China. *Palaeogeogr. Palaeoclimatol. Palaeoecol.* 528, 87–98. doi:10.1016/j.palaeo.2019.04.030

Zhang, Z., Yuan, X., Wang, M., Zhou, C., Tang, Y., Chen, X., et al. (2018). Alkaline-lacustrine deposition and paleoenvironmental evolution in permian Fengcheng Formation at the Mahu sag, Junggar Basin, NW China. *Pet. Explor. Dev.* 45, 1036–1049. doi:10.1016/S1876-3804(18)30107-1

Zhi, D., Tang, Y., He, W., Guo, X., Zheng, M., and Huang, L. (2021). Orderly coexistence and accumulation models of conventional and unconventional hydrocarbons in lower permian Fengcheng Formation, Mahu sag, Junggar Basin. *Pet. Explor. Dev.* 48, 43–59. doi:10.1016/S1876-3804(21)60004-6